Available online at www.sciencedirect.com

SciVerse ScienceDirect

Ceramics International 38 (2012) 6937–6941

CERAMICS INTERNATIONAL

www.elsevier.com/locate/ceramint

Short communication

Preparation and characterization of Eu^{3+}-doped fluorapatite nanoparticles by a hydrothermal method

Yuxiu Sun[a,*], Hua Yang[a], Dongliang Tao[b]

[a]*Tianjin Key Laboratory of Structure and Performance for Functional Molecules, College of Chemistry, Tianjin Normal University, Xiqing district binshui west road 393, Tianjin 300387, PR China*

[b]*College of Chemistry and Chemical Engineering, Fuyang Normal College, Anhui 236041, PR China*

Received 14 August 2011; received in revised form 10 May 2012; accepted 14 May 2012
Available online 22 May 2012

Abstract

In this study, luminescent Eu^{3+}-doped fluorapatite (Eu^{3+}:FA) was successfully synthesized by a hydrothermal process by using Na_2EDTA/citric acid (CA) as the chelating agent. X-ray diffraction (XRD), transmission electron microscopy (TEM) and photoluminescence spectra (PL) were utilized to characterize the obtained nanoparticles. The results showed that Eu^{3+} ions entered the FA lattice and occupied Ca^{2+} sites, which resulted in a decrease in the values of the lattice parameters. The as-prepared luminescent samples exhibit sphere-like aggregates that are constructed of small nanospheres and that are well dispersed with a good size distribution. Upon excitation by UV radiation, the Eu^{3+}:FA samples demonstrate the characteristic $^5D_0$–$^7F_{1-2}$ emission lines of Eu^{3+}. Finally, the influence of Na_2EDTA/CA on the morphology of Eu^{3+}:FA nanopowder was also discussed.

Keywords: Fluorapatite; Rare earth ions; Photoluminescence; Hydrothermal method

1. Introduction

Recently, calcium apatites [$Ca_{10}(PO_4)_6(OH, F, Cl)_2$], the principle inorganic components of bone and teeth, have been attracting significant interest in the fields of biomedicine, dental implants, catalysis and environment engineering, due to their bioactive, biocompatible and osteoconductive properties [1–5]. Among the family of calcium apatites, fluorapatite (FA) is considered an alternative biomaterial due to its low solubility and good biocompatibility in comparison to hydroxyapatite (HA) [6]. Additionally, calcium apatites can also be used in other fields. For example, trivalent rare-earth-ion-doped calcium apatites are employed as biological fluorescent probes due to their good luminescent properties [7]. Moreover, some cationic substitutions have potential applications in the fields of luminescence, water purification and bioceramics [8–10].

The trivalent ions of the 14 stable elements, from La through Lu, have ion radii ranging from slightly greater to slightly smaller than that of the Ca^{2+} ion. Moreover, having greater coordination numbers (generally greater than six) and showing little stereochemical preference in their coordination chemistry, Ln^{3+} ions exhibit a preference toward oxygen donor ligands, similar to the Ca^{2+} ion. In addition, the additional charge on Ln^{3+} ions is not a deterrent to their replacing Ca^{2+} [11].

Among the rare earth elements from La to Lu, Eu^{3+} ions have a simple electronic energy level scheme and hypersensitive transitions, which have been utilized extensively in color televisions and high-efficiency fluorescent lamps. The Eu^{3+}-doped calcium apatite is also believed to be a good biological probe candidate because of its more stable luminescence over time in comparison with fluorescent organic molecules [12–16] and its low toxicity and good biocompatibility [17]. Therefore, calcium apatites with the general formula $Ca_{10}(PO_4)_6(X)_2$ (X=OH or F) are good hosts for Eu^{3+} doping because Eu^{3+} has an ion radius similar to that of the Ca^{2+} in the calcium apatite lattice.

*Corresponding author. Tel.: +86 22 23766516.
E-mail address: hxxysyx@mail.tjnu.edu.cn (Y. Sun).

0272-8842/$36.00
http://dx.doi.org/10.1016/j.ceramint.2012.05.036

Thus far, many routes have been reported for the synthesis of rare-earth-doped apatite, including coprecipitation [18,19], the microemulsion-mediated hydrothermal process [20,21], the sol–gel combustion method [22], the thermal decomposition method [23], the high-temperature solid-state reaction [24] and microwave irradiation [25]. Nevertheless, some disadvantages exist for these processes, such as their time-consuming nature, the sophisticated effect parameters, chemical contamination, the microlevel particle size, the high reaction temperature and the high cost of the experimental equipment. Therefore, finding mild, facile and convenient synthesis procedures is quite advantageous. Moreover, there are few reports on the synthesis and characterization of Eu^{3+}-doped fluorapatite nanoparticles to our knowledge.

In this work, luminescent Eu^{3+}-doped fluorapatite {$Ca_{10}(PO_4)_6F_2$, Eu^{3+}:FA}was successfully synthesized via the chelating-reagent-assisted hydrothermal process. This research aims to prepare Eu^{3+}-doped fluorapatite nanoparticles using a more convenient process and to discuss the effects of Eu^{3+} incorporation into the structure of FA and Na_2EDTA/CA on the morphology of Eu^{3+}:FA nanoparticles.

2. Experimental

All the reagents were purchased without further purification. $Eu(NO_3)_3$ was obtained by dissolving stoichiometric Eu_2O_3 in dilute HNO_3 solution under vigorous stirring. The superfluous HNO_3 was driven off until the $Eu(NO_3)_3$ crystal powder was obtained.

2.1. Synthesis of Eu^{3+}:FA nanoparticles

In a typical experiment for the preparation of Eu^{3+}:FA nanoparticles, 0.7×10^{-3} mol of Na_2EDTA and 2.5×10^{-3} mol of CA were dissolved in distilled water. Under continuous stirring, 2.5×10^{-3} mol of $Ca(NO_3)_2$ and 2.5×10^{-5} mol of $Eu(NO_3)_3$ were added to the mixture, and a white emulsion-like mixture was obtained. Then, 1.5×10^{-3} mol of Na_3PO_4 and 0.5×10^{-3} mol of NaF were added to the above mixture, and a colorless and transparent solution was obtained. The pH value was adjusted to 5.0–5.8 by using 1 mol/L NaOH. The mixture was then transferred into a Teflon-lined stainless autoclave and kept at 160 °C for 12 h. The precipitates were separated by centrifugation and then dried in an oven at 70 °C for 6 h.

2.2. Characterization

Powder X-ray diffraction (XRD) patterns were obtained on a German Bruker AXS D8 ADVANCE diffractometer. The XRD data were recorded by using Cu K radiation ($\lambda=0.15406$ nm) at a scanning rate of 0.02°/s in the 2θ range from 20° to 60°. The obtained experimental patterns were compared with the standards compiled by the Joint Committee on Powder Diffraction and Standards (JCDPS), which involved card # 15-0876 for FA.

The crystallite size of the FA nanopowders was determined by using the Scherrer equation [26]

$$D_{hkl}=\frac{k\lambda}{B\cos}$$

where D is the crystallite size (nm), λ is the wavelength of the monochromatic X-ray beam (nm; $\lambda=0.154$ nm for Cu K radiation), θ is the diffraction angle (°), k is a constant varying with crystal habit and chosen to be 0.89 ($k=0.89$), and B is the full width at half maximum for the diffraction peak under consideration (rad). For this purpose, three diffraction peaks, (002), (202) and (222), which have the advantages of being well separated and having high intensities, were chosen for the measurement. The half-widths were calculated by the SigmaPlot software.

Lattice parameters (c and a) were calculated from peaks (002) and (211), respectively, using the standard HCP unit cell plane spacing relationship [27]

$$\frac{1}{d^2}=\frac{4}{3}\left(\frac{h^2+hk+k^2}{a^2}\right)+\frac{l^2}{c^2}$$

where d is the distance between adjacent planes in the set of Miller indices (hkl).

The photoluminescence spectrum of the sample was recorded with a Hitachi F-4500 Fluorescence Spectrophotometer at room temperature. Transmission electron microscope (TEM) images were recorded on an FEI Tecnai G2 S-Twin with an acceleration voltage of 200 kV.

3. Results and discussion

3.1. Phase structure analysis

In the present study, the composition of the synthetic Eu^{3+}-doped fluorapatite depends on the initial (Eu+Ca):P:F mole ratio in the starting solution. The designated extent of substitution of Ca^{2+} by Eu^{3+} was determined by the x value in the general formula of $Eu_xCa_{10-x}(PO_4)_6F_2$, where $x=0.1$. The atomic (Eu+Ca):P ratio was 1.67, which is the stoichiometric ratio of fluorapatite.

Fig. 1 shows the XRD patterns of Eu^{3+}:FA and the standard data for the hexagonal fluorapatite. Fig. 1(a) shows the XRD patterns of the Eu^{3+}:FA sample, wherein FA diffraction peaks were observed according to the standard card of FA (JCPDS #15-0876). No other metal oxide phases related to the doping component can be detected in the Eu^{3+}-doped calcium apatites. To clearly investigate the influence of the addition of Eu^{3+} in the FA crystallite, the lattice parameters of Eu^{3+}:FA powders are listed in Table 1.

The calculated lattice constants of the above samples are compared with those of the JCPDS no. 15-0876. It is shown that the calculated lattice constants of $a=b=0.9372$ nm and $c=0.6881$ nm are for Eu^{3+}:FA, and the standard

data of $a=b=0.9384$ nm and $c=0.6884$ nm are for standard FA. It is evident that Eu^{3+} ions (0.95 Å) entered the FA lattice and occupied Ca^{2+} (0.99 Å) sites, and the incorporation of Eu^{3+} ions into the fluorapatite resulted in the decrease of the lattice parameters.

The crystallite sizes of the prepared Eu^{3+}:FA sample calculated by using the XRD data are shown in Table 1. The crystallite size of the obtained powders is 33.3 nm.

3.2. TEM analysis

Fig. 2 shows the size and morphology of Eu^{3+}:FA powder samples obtained in the presence of Na_2EDTA/CA at 160 °C for 12 h. The morphology of the nanopowder indicates that it is composed of sphere-like agglomerates with narrow particle size distributions. In Fig. 2(a), the sizes of the agglomerates are in the range 30–46 nm. As observed at higher magnifications (Fig. 2(b)), these agglomerates are formed by nanoparticles with sphere-like shapes ranging from 5 to 9 nm.

This range is consistent with the crystallite size of Eu^{3+}:FA powders calculated by using XRD data within the error range.

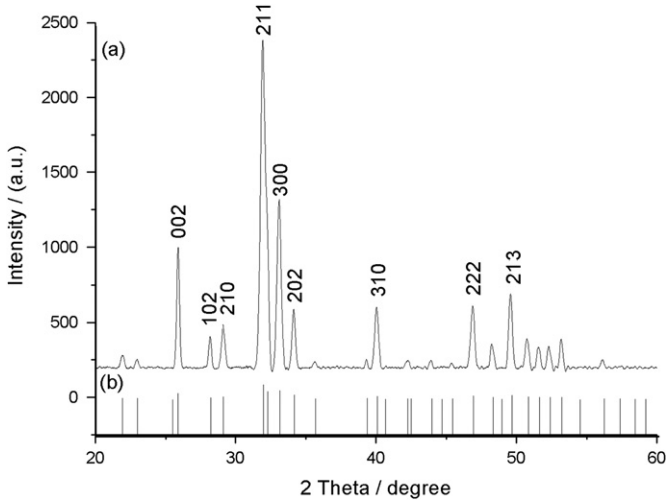

Fig. 1. XRD patterns of the synthetic Eu^{3+}-doped fluorapatite (a) and standard pure fluorapatite (b).

Table 1
Lattice parameters and crystallite size of the obtained powders.

Sample	*a*-axis (nm)	*c*-axis (nm)	Crystallite size (nm)
Eu^{3+}:FA	0.9372	0.6881	33.3
Standard FA	0.9384	0.6884	–

3.3. Photoluminescence properties

The emission spectrum of the Eu^{3+}:FA sample was recorded at an excitation wavelength of 250 nm, as shown in Fig. 3. The spectral features observed in the 582–603 nm and 603–640 nm ranges were ascribed to the Eu^{3+} ion $^5D_0 \rightarrow {}^7F_1$ and $^5D_0 \rightarrow {}^7F_2$ transitions, respectively. The

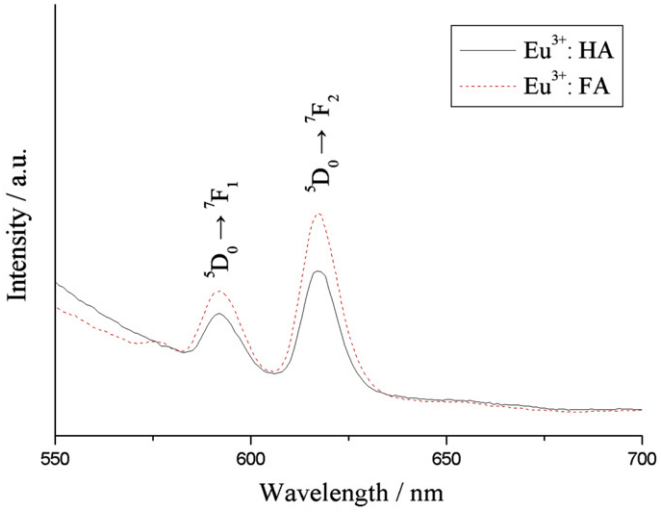

Fig. 3. Luminescence spectra of the Eu^{3+}:FA sample (dashed line) and the Eu^{3+}:HA sample (full line) (1% Eu^{3+} doping concentration, $\lambda_{ex}=250$ nm).

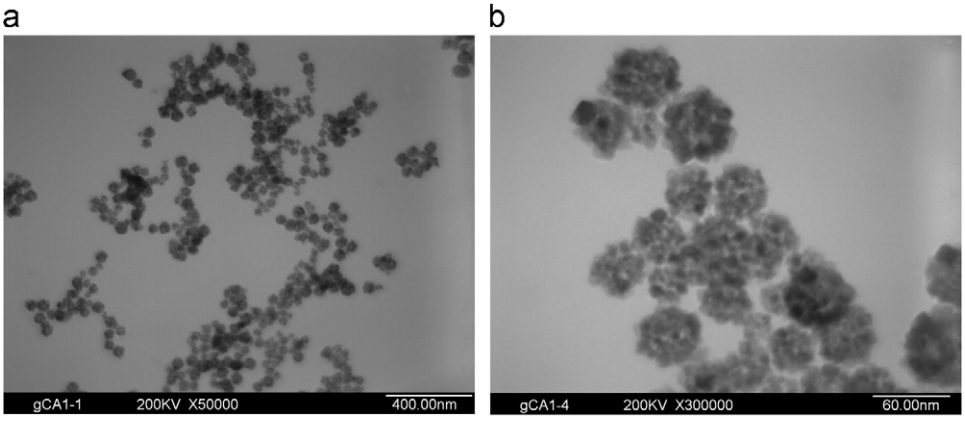

Fig. 2. (a) and (b) TEM images of Eu^{3+}:FA nanoparticles taken at different magnifications.

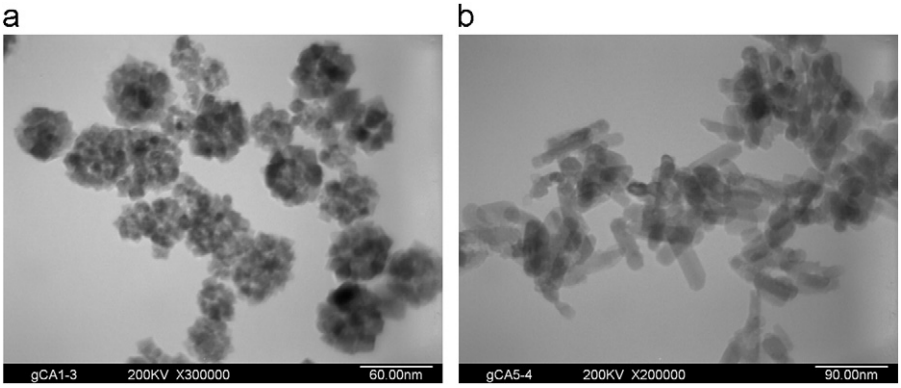

Fig. 4. TEM images of Eu^{3+}:FA nanoparticles obtained in the presence of Na_2EDTA/CA (a) and in the absence of Na_2EDTA/CA (b).

more efficient emission was observed for the hypersensitive $^5D_0 \rightarrow {}^7F_2$ transition with a maximum intensity at 617 nm.

We also found that the PL intensity of Eu^{3+}:FA increased slightly, in contrast to Eu^{3+}:HA sample, which was described in our recent report [19]. The comparison is based on the same Eu^{3+} doping concentration (1%), the same reaction time and temperature, and the fact that the chelating agent of CA/Na_2EDTA has no effect on the PL intensity in our present work. In addition, no significant modification of emission spectra was observed, expect for PL intensity. We believe that the increase of the PL intensity may be attributed to the replacement of OH^- by F^- in the structure of apatite crystals [28].

3.4. Effect of Na_2EDTA/CA

In our research, sphere-like Eu^{3+}:FA nanoagglomerates have been synthesized by a hydrothermal process by using CA and Na_2EDTA as chelating reagents. To investigate the effect of the chelating reagent on the Eu^{3+}:FA nanocrystals, Eu^{3+}:FA samples were also prepared in the absence of CA and Na_2EDTA.

Fig. 4(a) shows a typical TEM image of the sample obtained in the presence of Na_2EDTA/CA, which has a sphere-like morphology and is 30–46 nm in diameter. Fig. 4(b) shows the sample obtained in the absence of Na_2EDTA/CA. It is evident that rod-like Eu^{3+}:FA nanoparticles 48–69 nm in length and 16–25 nm in width were produced when Na_2EDTA/CA was not present, while sphere-like aggregates were obtained by using Na_2EDTA/CA as a chelating reagent. It is believed that citric species could promote the aggregation of apatite nanoparticles in a side-by-side manner due to the electrostatic attraction between the $-COO^-$ groups and the calcium ions [29]. In our case, Na_2EDTA/CA may be absorbed on the surface of Eu^{3+}:FA crystals and prevent crystal growth along the *c*-axis. In addition, in the CA-enriched solution, to reduce the surface energy, sphere-like Eu^{3+}:FA nanocrystals with a higher energy would assemble together rapidly to form the sphere-like aggregates.

4. Conclusions

In summary, luminescent Eu^{3+}-doped fluorapatite (Eu^{3+}:FA) was successfully synthesized by a hydrothermal process by utilizing Na_2EDTA and CA as the growth control agents. The incorporation of Eu^{3+} ions into the fluorapatite resulted in a decrease in the values of the lattice parameters. The as-prepared luminescent samples exhibit sphere-like aggregates that are constructed of small nanospheres. Upon excitation by UV radiation, the Eu^{3+}:FA samples demonstrate the characteristic $^5D_0 \rightarrow {}^7F_{1-2}$ emission lines of the Eu^{3+} ion. The influence of Na_2EDTA/CA on the morphology of Eu^{3+}:FA crystals may be attributed to the fact that in the CA-enriched solution, to reduce the surface energy, sphere-like Eu^{3+}:FA nanocrystals with higher energy would assemble together rapidly to form the sphere-like aggregates.

Acknowledgments

This project is financially supported by the National Natural Science Foundation of China (NSFC 20803052, 51102180) and Tianjin Normal University Doctoral Foundation (52X09007).

References

[1] R.Z. LeGeros, Calcium Phosphates in Oral Biology and Medicine, Karger, Basel, Switzerland, 1991.
[2] M. Mazaheri, M. Haghighatzadeh, A.M. Zahedi, S.K. Sadrnezhaad, Effect of a novel sintering process on mechanical properties of hydroxyapatite ceramics, Journal of Alloys and Compounds 471 (2009) 180–184.
[3] M. Kheradmandfard, M.H. Fathi, Preparation and characterization of Mg-doped fluorapatite nanopowders by sol–gel method, Journal of Alloys and Compounds 504 (2010) 141–145.
[4] M. Descamps, J.C. Hornez, A. Leriche, Manufacture of hydroxyapatite beads for medical applications, Journal of the European Ceramic Society 29 (2009) 369–375.
[5] A. Bianco, I. Cacciotti, M. Lombardi, L. Montanaro, E. Bemporad, M. Sebastiani, F-substituted hydroxyapatite nanopowders: thermal stability, sintering behavior and mechanical properties, Ceramics International 36 (2010) 313–322.

[6] H.B. Qu, M. Wei, The effect of fluoride contents in fluoridated hydroxyapatite on osteoblast behavior, Acta Biomaterialia 2 (2006) 113–119.
[7] A. Lebugle, F. Pelle, C. Charvillat, I. Rousselot, J.Y. Chane-Ching, Colloidal and monocrystalline Ln^{3+} doped apatite calcium phosphate as biocompatible fluorescent probes, Chemical Communications 6 (2006) 606–608.
[8] E. Boanini, P. Torricelli, M. Gazzano, R. Giardinob, A. Bigi, Alendronate-hydroxyapatite nanocomposites and their interaction with osteoclasts and osteoblast-like cells, Biomaterials 29 (2008) 790–796.
[9] X. Chen, T. Wu, Q. Wang, J.W. Shen, Shield effect of silicate on adsorption of proteins onto silicon-doped hydroxyapatite (100) surface, Biomaterials 29 (2008) 2423–2432.
[10] J.K. Liu, Q.S. Wu, Y.P. Ding, Self-assembly and fluorescent modification of hydroxyapatite nanoribbon spherulites, European Journal of Inorganic Chemistry (2005) 4145–4149.
[11] D. William, Horrocks Jr, Daniel R. Sudnick, Lanthanide ion luminescence probes of the structure of biological macromolecules, Accounts of Chemical Research 14 (1981) 384–392.
[12] R. Ternane, M. Trabelsi-Ayedi, N. Kbir-Ariguib, B. Piriou, Luminescence properties of Eu^{3+} in calcium hydroxyapatite, Journal of Luminescence 81 (1999) 165–170.
[13] A.A. Bol, A. Meijerink, Long-lived Mn^{2+} emission in nanocrystalline ZnS:Mn^{2+}, Physical Review B 58 (1998) R15997–R16000.
[14] A. Doat, M. Fanjul, F. Pelle, E. Hollande, A. Lebugle, Europium-doped bioapatite: a new photostable biological probe, internalizable by human cells, Biomaterials 24 (2003) 3365–3371.
[15] A. Doat, F. Pelle, A. Lebugle, Europium-doped calcium pyrophosphates: allotropic forms and photo luminescent properties, Journal of Solid State Chemistry 178 (2005) 2354–2362.
[16] A. Doat, F. Pelle, N. Gardant, A. Lebugle, Synthesis of luminescent bioapatite nanoparticles for utilization as a biological probe, Journal of Solid State Chemistry 177 (2004) 1179–1187.
[17] C.S. Ciobanu, F. Massuyeau, E. Andronescu, M.S. Stan, A. Dinischiotu, D. Predoi, Biocompatibility study of europium doped crystalline hydroxyapatite bioceramics, Digest Journal of Nanomaterials and Biostructures 6 (2011) 1639–1647.
[18] P. Yang, Z. Quan, C. Li, X. Kang, H. Lian, J. Lin, Bioactive luminescent and mesoporous europium-doped hydroxyapatite as a drug carrier, Biomaterials 29 (2008) 4341–4347.
[19] S.P. Mondejar, A. Kovtun, M. Epple, Lanthanide-doped calcium phosphate nanoparticles with high internal crystallinity and with a shell of DNA as fluorescent probes in cell experiments, Journal of Materials Chemistry 17 (2007) 4153–4159.
[20] C. Yang, P. Yang, W. Wang, J. Wang, M. Zhang, J. Lin, Solvothermal synthesis and characterization of Ln (Eu^{3+},Tb^{3+}) doped hydroxyapatite, Journal of Colloid and Interface Science 328 (2008) 203–210.
[21] Y. Sun, H. Yang, D. Tao, Microemulsion process synthesis of lanthanide-doped hydroxyapatite nanoparticles under hydrothermal treatment, Ceramics International 37 (2011) 2917–2920.
[22] Y. Han, X. Wang, S. Li, X. Ma, Synthesis of terbium doped calcium phosphate nanocrystalline powders by citric acid sol–gel combustion method, Journal of Sol–Gel Science and Technology 49 (2009) 125–129.
[23] M. Long, F. Hong, W. Li, F. Li, H. Zhao, Y. Lv, H. Li, F. Hu, L. Sun, C. Yan, Z. Wei, Size-dependent microstructure and europium site preference influence fluorescent properties of Eu^{3+}-doped $Ca_{10}(PO_4)_6(OH)_2$ nanocrystal, Journal of Luminescence 128 (2008) 428–436.
[24] J. Zhang, H. Liang, R. Yu, H. Yuan, Q. Su, Luminescence of Ce^{3+}-activated chalcogenide apatites $Ca_{10}(PO_4)_6Y$ (Y=S,Se), Materials Chemistry and Physics 114 (2009) 242–246.
[25] C. Yang, P. Yang, W. Wang, S. Gai, J. Wang, M. Zhang, J. Lin, Synthesis and characterization of Eu-doped hydroxyapatite through a microwave assisted microemulsion process, Solid State Sciences 11 (2009) 1923–1928.
[26] B.D. Cullity, Elements of X-ray diffraction, 2nd ed., Addison-Wesley publishing, 1977, p. 284.
[27] T.J. Webster, E.A. Massa-Schlueter, J.L. Smith, E.B. Slamovich, Osteoblast response to hydroxyapatite doped with divalent and trivalent cations, Biomaterials 25 (2004) 2111–2121.
[28] A.N. Trukhin, K. Smits, A. Sharakosky, G. Chikvaidze, T.I. Dyuzheva, L.M. Lityagina, Luminescence of dense, octahedral structured crystalline silicon dioxide (stishovite), Journal of Luminescence 131 (2011) 2273–2278.
[29] M.A. Martins, C. Santos, M.M. Almeida, M.E.V. Costa, Hydroxyapatite micro and nanoparticles: nucleation and growth mechanisms in the presence of citrate species, Journal of colloid and interface science 318 (2008) 210–216.